

CHARACTERISTICS OF TRANSITIONAL AND TURBULENT JET DIFFUSION FLAMES IN MICROGRAVITY*

M. Yousef Bahadori[†] and James F. Small, Jr.
Science Applications International Corporation
Torrance, California 90501

Uday G. Hegde,[‡] Liming Zhou,[§] and Dennis P. Stocker
NASA Lewis Research Center
Cleveland, Ohio 44135

Introduction

This paper presents the ground-based results obtained to date in preparation of a proposed space experiment to study the role of large-scale structures in microgravity transitional and turbulent gas-jet diffusion flames, by investigating the dynamics of vortex/flame interactions and their influence on flame characteristics. The overall objective of this effort is to gain an understanding of the fundamental characteristics of transitional and turbulent gas-jet diffusion flames. Understanding of the role of large-scale structures on the characteristics of microgravity transitional and turbulent flames will ultimately lead to improved understanding of normal-gravity turbulent combustion.

Ground-based experiments conducted in this program have revealed significant differences between normal-gravity and microgravity flames (e.g., refs. 1 and 2). For example, microgravity transitional and turbulent flames are dominated by the formation and convection of large-scale structures and their interaction with the flame. Although large-scale structures are an integral part of turbulent flames in normal gravity as well, their evolution and interaction with the flame is completely different. In particular, buoyant acceleration in normal gravity promotes the formation of small scales, even at low cold-jet Reynolds numbers, which interact with the flame and with the large-scale structures. In microgravity, buoyantly induced formation of small scales is absent. Hence, microgravity gas-jet diffusion flames are dominated by large-scale structures over a significant range of Reynolds numbers. This does not imply that these flames contain a single, well-defined turbulent scale. Nor does it imply that the dynamics of disturbances are non-random. In fact, observations to date from drop-tower tests conducted in this program show that the transitional and turbulent microgravity flames contain randomly generated large-scale structures which exhibit symmetric and/or asymmetric characteristics, and therefore, have multiple instability modes. The effects of microgravity on transitional and turbulent flames is to increase the size of the smallest scales (i.e., the Kolmogorov scale) compared to the normal-gravity case (ref. 2). However, even in microgravity, the problem of multiple, interacting large scales and modes persists. In order to understand the cause of the observed behavior of transitional and turbulent diffusion flames in microgravity, one approach is to separate the effects of these interacting modes and scales by studying the response of a microgravity flame to a single mode with one time scale and one length scale.

The proposed space experiment is aimed at the effects of the structure parameters (e.g., frequency, amplitude) responsible for the observed characteristics of transitional and turbulent gas jet diffusion flames. In order to achieve this objective, large-scale, controlled disturbances are imposed on a well-defined microgravity laminar diffusion flame. Similar techniques have been used in the past in order to study the characteristics of transitional and turbulent shear layers, and to understand the interaction of vortical structures with the flame (e.g., ref. 3). A normal-gravity, laminar gas-jet diffusion flame cannot be utilized for this purpose due to buoyantly induced hydrodynamic instabilities which cause flame oscillations and introduce additional length and time scales (e.g., ref. 4). Implicit in most normal-gravity combustion models is the assumption that the behavior of the smallest scales of turbulence can be related in a specific and universal way to correlations obtained from the characteristics of large-scale structures (ref. 5). In normal-gravity, however, as Grashof number estimates clearly show (ref. 6), buoyancy profoundly influences the large scales whereas it has no effect on the smallest scales (smaller than approximately 100 microns; see ref. 6). On the other hand, in microgravity, there is no buoyant influence on the large scales. Therefore, modeling of the small scales of turbulence based on the properties of the large scale structures in microgravity will not be contaminated by buoyancy, leading to improved turbulent combustion models applicable in normal gravity.

* Paper presented at the Third International Microgravity Combustion Conference, April 11-13, 1995, Cleveland, Ohio. This work is supported by NASA Lewis Research Center under Contract NAS3-25982 (start date: November 11, 1991) with SAIC.

[†] Author for correspondence; Thermal Sciences Division, 21151 Western Avenue.

[‡] NYMA, Inc., NASA Lewis Research Center Group, Brook Park, Ohio.

[§] Analix Corp., NASA Lewis Research Center Group, Brook Park, Ohio.

Laminar/Transitional/Turbulent Flames in Microgravity

The classical behavior of laminar/transitional/turbulent gas-jet diffusion flames in normal gravity is shown by Hottel and Hawthorne (ref. 7). References 1 and 2 show that fundamental differences, such as flame height behavior with Reynolds number, onset of instabilities, extent of the transitional regime, and blow-off limit characteristics exist between the normal-gravity and microgravity flames. Thus, a major finding of this work is that buoyancy has a significant effect on these gas-jet flames regardless of the Reynolds number regime (Fig. 1). The microgravity experiments were conducted at the 2.2-second Drop Tower at the NASA Lewis Research Center. Several hydrocarbon fuels were employed with fuel being injected into quiescent air at atmospheric pressure through a nozzle of 0.45 to 1.65 mm in diameter. The cold-jet Reynolds number, based upon the nozzle diameter and inlet velocity, covered the entire range of laminar, transitional, and turbulent (up to $Re = 9000$). Both the normal-gravity and microgravity laminar flames exhibit a linear increase in luminous height with increasing jet momentum and Reynolds number. However, the microgravity flame is taller and wider than the corresponding normal-gravity flame for all regimes. Furthermore, the microgravity flames are less luminous, but due to the larger size and accumulation of hot products, they radiate up to an order of magnitude more than flames in normal gravity (ref. 8).

The transitional regime in normal gravity jet diffusion flames is characterized by the appearance of instabilities at the flame tip (at $Re \sim 2300$; see Fig. 1). The location of the onset of instability moves upstream toward the nozzle as the jet Reynolds number is increased, with the lower part of the flame maintaining its laminar characteristics. In addition, the height of the flame starts to decrease due to the enhancement of mixing caused by instabilities. Thus, the flame becomes wrinkled, increasing in surface area which increases the total transport per unit length of the flame, thereby shortening the overall flame length. Microgravity flames have been observed to be laminar for Reynolds numbers up to ~ 2000 (ref. 9). Transition in the observed microgravity flames (refs. 1 and 2) is characterized by the appearance of intermittent, naturally occurring disturbances which are generated near the flame base and are convected downstream (in contrast to the normal-gravity flames where disturbances are first observed at the flame tip). Between two successive disturbances, the flame appears laminar and undisturbed. As the jet Reynolds number increases, the frequency of occurrence of the disturbances increases. Above Reynolds number of approximately 3000, a continuous train of disturbances is formed and is convected downstream along the flame (see Fig. 1). The disturbances distort the flame as they move downstream. An important effect is their influence on the flame tip. In the laminar regime, microgravity propane flames exhibit (apparent) open tips. However, the tip tends to close when the disturbances arrive at the tip. When there is a continuous train of disturbances (i.e., in the turbulent regime), the tip closing is permanent. The height of the transitional and turbulent microgravity flames continues to increase with injection Reynolds number until near-blowoff conditions, although at a slower rate compared to the variation in the laminar regime. Note that at the higher Reynolds number (3500 and above), the normal-gravity flame height is almost constant, indicating that turbulent conditions have been achieved, whereas the microgravity flame height is still increasing (see Fig. 1). The decrease in the normal-gravity flame height as transition to turbulence commences is believed to be caused by increased turbulent transport which opposes the tendency for increased flame height due to increased jet momentum.

The correlation for turbulent flame height, H , has been traditionally established by using the laminar flame relation $H_L \sim Q/D$ and substituting the turbulent diffusivity, D_{eff} , for the molecular diffusivity D . Here, H_L is the laminar flame height and Q is the fuel volume flow rate. Furthermore, D_{eff} is assumed (ref. 10) to be proportional to the product of nozzle diameter, d , and jet exit velocity, u_0 , i.e., $D_{eff} \sim u_0 d$. This leads to the conclusion that the flame height in the turbulent regime is independent of the fuel flow rate and is linearly proportional to the nozzle diameter alone, that is, $H \sim d$. It would be expected that as the injection Reynolds number increases, the relative importance of forced convection would increase and the dependence on buoyancy would decrease. Thus, defining the Froude number (in terms of the injection velocity u_0 , flame height H , and gravitational acceleration g) by $Fr = u_0^2/gH$, which denotes the ratio of forced convection and buoyant convection, it may be expected that as Fr becomes large, gravity effects become small. However, our studies show that the behavior of normal-gravity turbulent flames with Froude numbers in excess of 100 remains substantially different than the behavior of their microgravity counterparts. In particular, the continual increase in the microgravity flame height in the transitional and turbulent Reynolds number ranges indicates that any increased transport due to the effect of the naturally occurring disturbances does not fully overcome the effects of increased jet momentum, as in normal gravity. An estimate of the effective diffusivity in the microgravity transitional/turbulent regime may be obtained by assuming that the laminar-flame relation $H_L \sim Q/D$ holds with D replaced by the effective diffusivity D_{eff} . This yields the result that D_{eff} for the normal-gravity flames is approximately three times the value of D_{eff} for the microgravity flame (ref. 2). One reason for this difference in the values of D_{eff} in microgravity and normal gravity is due to the preferential generation of smaller scales in normal gravity compared to microgravity. Large scales are not very effective in the fine-scale mixing process (required to enhance combustion rates and reduce flame height for a given flow rate) since their action is primarily to move packets of fluid from one location to another. Small scales, on the other hand, enhance local mixing, thereby increasing the effective diffusivity of fuel and oxidizer at the flame.

Additionally, in the normal-gravity turbulent flames, the base lifts off the nozzle tip, and air entrainment creates a premixed region at the base of the flame, resulting in flame stabilization at a standoff location where the flame velocity balances the local flow velocity (see Fig. 1). As the jet momentum increases beyond a critical value, this balance is no longer sustainable, resulting

in flame blowoff. For turbulent microgravity flames, our studies (ref. 1) have shown that flame standoff distance is approximately 50% of that for the corresponding normal-gravity flame. This suggests that even at the base of the flame, buoyancy plays an important role in determining flame characteristics. Closely related to flame standoff is the blowoff limit. For microgravity flames, the blowoff Reynolds number is substantially higher than that of the flames in normal gravity (see Fig. 1). Near the blowoff Reynolds number, the microgravity standoff distance begins to increase, and the flame takes on a premixed appearance, and flame height begins to decrease, as shown in Fig. 1. Further increase in the Reynolds number results in blowoff in microgravity.

Vortex-Flame Interactions in Microgravity

The proposed space experiment utilizes the interaction of controlled disturbances with a laminar gas jet diffusion flame in microgravity in order to understand the fundamental vortex-flame interactions and their effects on the observed behavior of microgravity transitional and turbulent flames. The basis for this approach lies in the connection between the imposed and naturally occurring disturbances (see ref. 2), where spatial instability theory is applicable to a jet under the action of both types of disturbances for arbitrary Reynolds numbers. Therefore, imposing a harmonic disturbance on a microgravity laminar gas jet diffusion flame creates effects similar to those occurring naturally in transitional and turbulent diffusion flames observed in microgravity; this has been discussed in detail elsewhere (ref. 2).

A sinusoidally-driven iris is used to provide well-defined and controlled disturbances to interact with the flame. The plane of the iris is mounted approximately 5 mm above the nozzle tip, with its center coincident with the nozzle axis. Harmonic axisymmetric disturbances are obtained by periodically opening and partially closing the iris at 0-10 Hz. The difference between the maximum and minimum diameters of the iris (2.2 and 1.2 cm) during the pulsing is a measure of the amplitude of the disturbance. The average iris opening, amplitude and oscillation frequency define the shear-layer pulsations that are imposed on the jet flow. These disturbances have been characterized by LDV measurements under isothermal (non-reacting) conditions.

The disturbance technique has been tested on flames in the Zero-G Facility with satisfactory results. In these 5.18-second, microgravity tests, propane (at 2 cc/sec and $Re \approx 350$, based on nozzle diameter and cold-jet properties) is injected in quiescent air, and then ignited by a hot wire. The experiment chamber is equipped with thermocouples, both slice and global radiometers, a pressure transducer, a retractable ignitor, and two cameras.

Modeling

Modeling is an integral part of the program, and is needed to interpret the experimental results and improve our understanding of the fundamental mechanisms that occur in microgravity diffusion flames. The proposed space experiment utilizes a pulsed laminar flame in microgravity. Hence, a linearized analytical model is developed for the effects of imposed pulsations on the flame. Extensions to the linearized model to include non-linear terms are underway. In addition, a transient Navier-Stokes numerical model is utilized to predict the characteristics of microgravity flames under the effects of imposed pulsations.

The analytical model of the pulsed laminar flames in microgravity treats the effects of a harmonic source localized at the flame base. This simulates the naturally occurring disturbances observed to originate at the base. However, in contrast to the transitional and turbulent flames which exhibit a multiplicity of scales, the pulsed laminar flame is subjected to a disturbance of single characteristic length and time scales, in accordance with the proposed space experiment. Using this approach, the effects of the parameters of the disturbance on flame behavior can be studied. Once the effects of a single-type disturbance are identified, the model will be extended for multiple-disturbance types with arbitrary modes and scales. The analytical model is comprised of linearized, time-dependent conservation equations. It allows for both radial and axial variations of the mean velocity and temperature. The disturbances may be axisymmetric or asymmetric, and are characterized by their frequency and amplitude. A closed-form representation of the time-dependent flame shape variation is obtained by invoking the flame sheet approximation. Results are obtained for instantaneous flame shape under the action of an axisymmetric disturbance near the base of the flame, as shown in Fig. 2. As seen, the wavelength of the disturbance decreases as it is convected downstream. This is due to the higher velocities near the base of the flame and lower velocities downstream for microgravity flames, as predicted elsewhere (ref. 11). The analysis will be modified to include non-linear, second-order effects (such as mode-mode interactions).

A comprehensive transient, Navier-Stokes model is utilized to predict the characteristics of the flame under the influence of disturbances. The model provides pressure, velocity, temperature, and species fields in the presence of convective, conductive, and radiative heat transfer. Predictions such as the following will be compared with experimental data and observations to validate the model: (i) both time-averaged and oscillatory flame shapes; (ii) convection velocity of the structures; (iii) size variations of the structures along the flame; (iv) both time-averaged and oscillatory temperature fields. Once the model is validated, it will also be used to determine the effects of oscillations on radiation and effective transport properties for flames in the presence of a disturbance.

Results and Discussion

Unpulsed Flame: The centerline temperature of microgravity flame drops with increase in axial distance (see Fig. 3) in contrast to normal-gravity flames where the temperature drops only beyond the tip. Predictions have confirmed this behavior, as shown in Fig. 4. The temperatures in the downstream portion of the flame in Fig. 3 were still increasing at the end of the drop with those near the tip registering an increase at the rate of approximately 75 K/sec. Whereas the thermocouple closer to the nozzle exit has shown steady-state temperature data, the thermocouple near the flame tip has indicated that the upper part of the flame is still in transient state.

Tests were conducted with the global radiometers placed at different axial locations above the nozzle tip. The radial location in all cases was 10 cm from the nozzle centerline. Figure 5 plots the radiometer signals at four locations ($x = 2, 4.5, 9.5,$ and 12 cm) during the last 1.5 seconds of the drop. It is seen that the highest signal is obtained at $x = 4.5$ cm which corresponds to x/L of approximately 0.45. Good agreement between predictions and data (from the last instant of the drop) for the global radiometer measurements is obtained (see Fig. 6). The predicted flame radiation shown in Fig. 6 indicates that the optimum axial location for the global radiometer in terms of the signal strength is between $0.40 < x/L < 0.55$ for the microgravity case where L is the flame length. The calculations assumed that the radiometer was located at a radial distance of 10 cm from the flame centerline consistent with the design of the proposed flight experiment. The optimum signal strength occurs a little below half-height of the flame due to the drop in flame temperature with axial distance when radiation is taken into account. The discrepancy between measurements and predictions in the upper half of the flame in Fig. 6 is due to the transient nature of radiation (see Fig. 5), as discussed below, since the predicted values are from the steady state model. Clearly, the observed increase which persists after 5 seconds of microgravity in these signals is due to increasing amounts of hot gases in the field of view of the radiometers. Estimates based upon radial diffusion suggest that the near-field of the flame will approach steady conditions after about 15 seconds of burning. However, the continuous accumulation of products may begin to affect oxidizer transport to the flame, particularly near the tip region. If this occurs, combustion near the tip may be reduced, resulting in a possible drop in thermal radiation as the production of hot gases is reduced. Pulsing and consequent increased entrainment of oxidizer into the flame may reverse this effect.

The unpulsed flame studies show the following: (a) Temperatures near the flame tip are increasing by 75 K/sec at the end of the drop (not shown here); (b) Global radiometer signals are increasing at a rate of 15% per second at the end of the drop, see Fig. 5; (c) Slice radiometer signals (not shown here) are increasing at a rate of 5% per second at the end of the drop; (d) Optimum location of the global radiometer is verified to be at $x/L \sim 0.45$, which is consistent with numerical calculations, see Fig. 6; (e) Temperature drop along the centerline of the microgravity flames is verified both experimentally (see Fig. 3) and numerically (see Fig. 4); and (f) Microgravity times longer than 5 seconds are needed to approach steady conditions in the near-field of the flame.

Pulsed Flame: The pulsed-flame studies in the Zero-G Facility were conducted for iris frequencies of 2.5, 5.0, and 7.5 Hz, with fuel flow rate of 2 cc/sec. Figure 7 shows the oscillatory centerline temperature at two axial locations for $f = 2.5$ Hz during the last two seconds of the drop. Sinusoidal variations in temperature data are obtained, since the iris is pulsed sinusoidally in this experiment. Temperature oscillations are strongest near the base of the flame. The oscillatory temperature data at different radial locations (at the centerline and near the flame) for the same axial location are shown in Fig. 8 for $f = 2.5$ Hz during the last two seconds of the drop. The data show that temperature oscillations are out of phase at the two locations due to vortex dynamics. The slice radiometer signals display the sinusoidal nature of these oscillations, as shown in Fig. 9 for two axial locations of the radiometer at $f = 2.5$ Hz during the last two seconds of the test. The centerline temperature autospectra show that the dominant frequency is the iris pulsation frequency. In addition, it is found that the centerline temperature-oscillation amplitude is smaller at higher frequencies and drops in the axial direction. Temperature coherence and slice radiation-temperature coherence of 0.95 to 1.00 are obtained from these tests.

The pulsed microgravity flame studies can be summarized as follows: (a) Iris pulsing leads to sinusoidal temperature and radiation oscillations, see Figs. 7-9; (b) Centerline temperature amplitude decreases with axial distance, which indicates damping of the disturbances; see Fig. 7; (c) Increasing the pulse frequency (results not shown here) decreases the amplitude of the centerline temperature oscillations; (d) Temperature oscillations near the centerline are 180° out of phase with oscillations near the flame sheet, which is consistent with vortex dynamics, see Fig. 8; (e) Near-perfect coherence of ≈ 1 between both temperature and radiation oscillations are observed over the flame length (results not shown here), which is not observed in normal gravity; (f) Time-averaged data do not reach near-steady state in 5 seconds of microgravity, see, e.g., Fig. 7; and (g) 5 seconds of microgravity does not provide enough time to obtain statistically stationary data.

Conclusion

The microgravity tests conducted for the laminar, transitional and turbulent regimes show significant differences compared to flames in normal gravity. These include flame height behavior with Reynolds number, onset of instabilities, extent of the transitional regime, and flame stand-off and blow-off behavior. In order to gain a better understanding of characteristics of these flames, microgravity tests in preparation of a space flight experiment were conducted on the effects of imposed disturbances on a laminar diffusion flame. The tests provided data such as flame centerline temperature distribution, optimum radiometer location, temperature and radiation oscillations due to flame/disturbance interactions, and effects of imposed oscillation frequency on flame properties. The results also show that 5 seconds of microgravity is not sufficient to approach near-field steady conditions in the unpulsed or (time-averaged) pulsed flames, and to obtain statistically stationary data for the pulsed case.

References

1. Bahadori M.Y., Stocker D.P., Vaughan D.F., Zhou L., and Edelman R.B. (1993), Modern Developments in Energy, Combustion, and Spectroscopy, pp. 49-66. (F.A. Williams, A.K. Oppenheim, D.B. Olfe, and M. Lapp, eds.), Pergamon Press, New York.
2. Hegde U.G., Zhou L., and Bahadori M.Y. (1995), Combust. Sci. Tech., in press.
3. Markstein G.H. (1949), Third Symposium on Combustion, pp. 162-167, Williams and Wilkins Co., Baltimore, Maryland.
4. Strawa A.W. and Cantwell B.J. (1985), Phys. Fluids, 28 (8), 2317-2320.
5. Peters N. (1986), 21st Symposium (International) on Combustion, pp. 1231-1250, The Combustion Institute, Pittsburgh, Pennsylvania.
6. Faeth G.M. (1991), Homogeneous premixed and nonpremixed flames in microgravity: a review. AIAA/IKI Meeting, Moscow, USSR. American Institute of Aeronautics and Astronautics.
7. Hottel H.C. and Hawthorne W.R. (1949), Third Symposium on Combustion, pp. 254-266, Williams and Wilkins Co., Baltimore, Maryland.
8. Bahadori M.Y., Edelman R.B., Sotos R.G., and Stocker D.P. (1991), Radiation from gas-jet diffusion flames in microgravity environments. Paper AIAA-91-0719, AIAA 29th Aerospace Sciences Meeting, Reno, Nevada.
9. Zhou L., Hegde U.G., and Bahadori M.Y. (1992), Reduced-gravity observations of high-momentum laminar diffusion flames. Western States Meeting of The Combustion Institute, Berkeley, California.
10. Hawthorne W.R., Weddell D.S., and Hottel H.C. (1949), Third Symposium on Combustion, pp. 266-288, Williams and Wilkins Co., Baltimore, Maryland.
11. Edelman R.B. and Bahadori M.Y. (1986), Acta Astronautica, 13, 681-688.

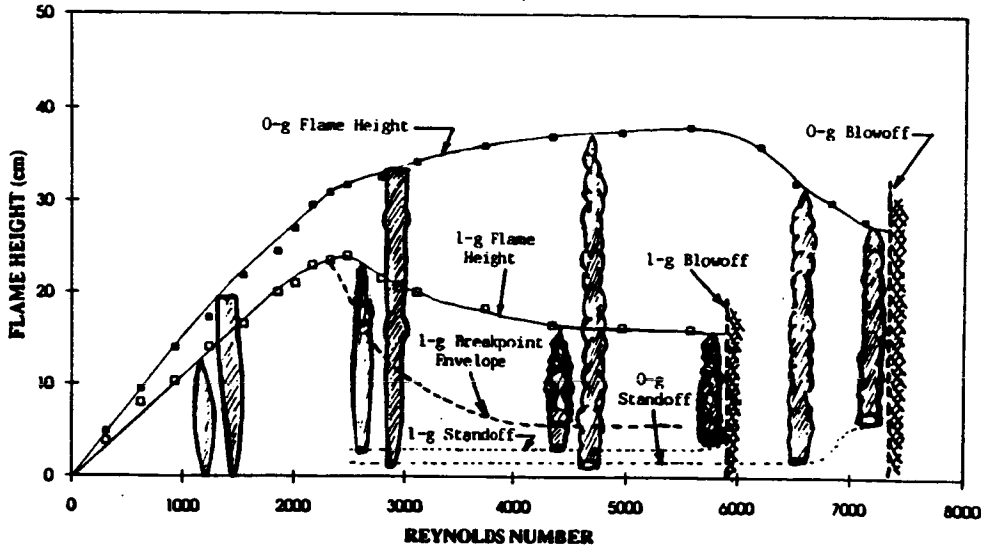


Fig. 1. Microgravity and normal-gravity heights of propane flames burning in quiescent air at 1 atm, as a function of the jet Reynolds number (based on fuel properties and nozzle diameter); nozzle diameter = 0.8 mm.

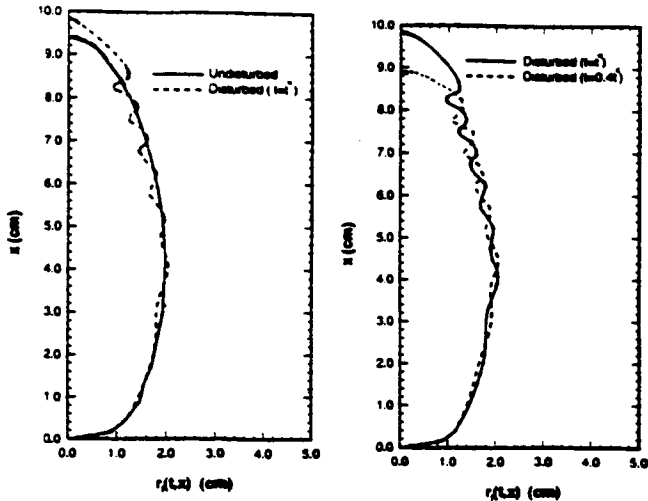


Fig. 2. Predicted instantaneous flame shape under the action of an axisymmetric disturbance mechanism located near the base of the flame. Flame shapes are shown for disturbed ($t = t^*$ and $t = 0.4 t^*$) and undisturbed cases.

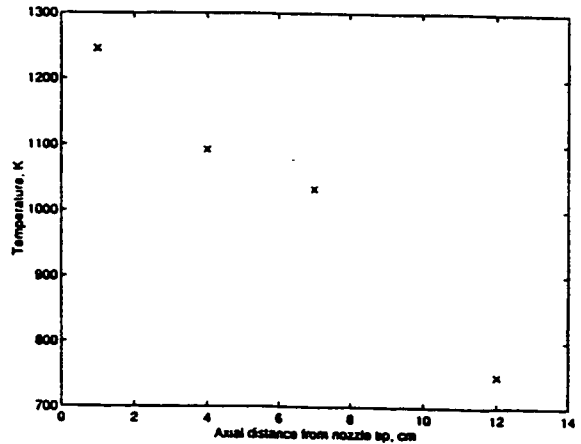


Fig. 3. Axial variation of centerline temperature for undisturbed microgravity flame of propane at 2 cc/sec. Note that the thermocouple signal for $x = 1$ cm saturated due to a limitation of the data acquisition system in the zero-g drop rig. Hence, the temperature at this location is higher than shown. The luminous flame height was between 10-11 cm.

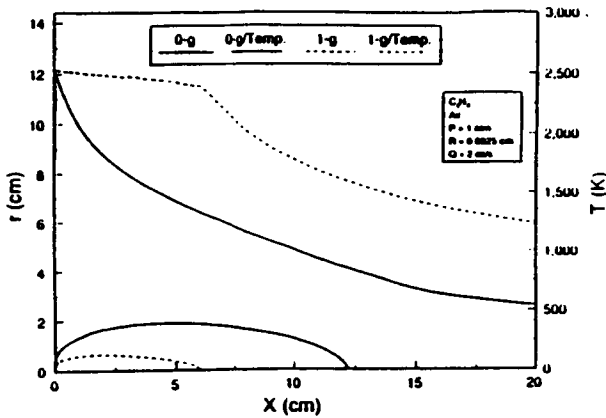


Fig. 4. Predicted flame shape and centerline temperature for both normal-gravity and microgravity flames of propane.

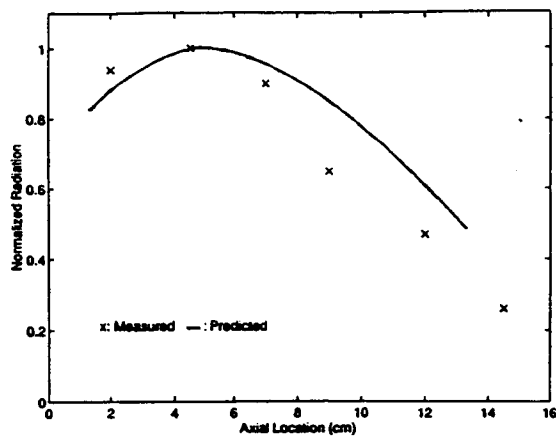


Fig. 6. Measured and predicted flame global radiation as a function of radiometer axial location for a radial location of 10 cm. The microgravity propane flame has a volume flow rate of 2 cc/sec.

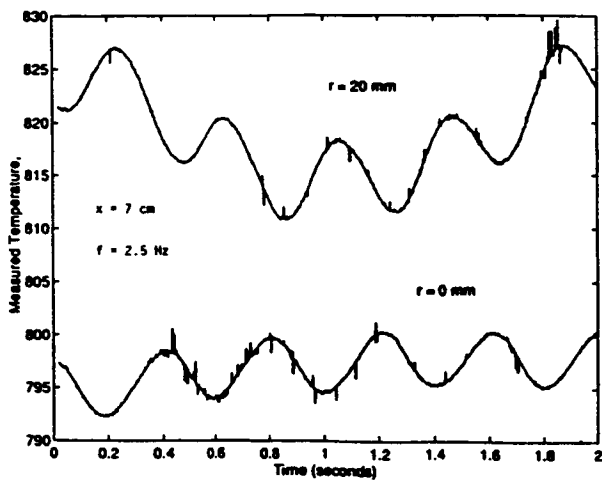


Fig. 8. Temperature during the last two seconds of the drop for two radial locations (i.e., centerline and near the flame) at axial location of 7 cm; microgravity propane flame at 2 cc/sec; iris frequency = 2.5 Hz.

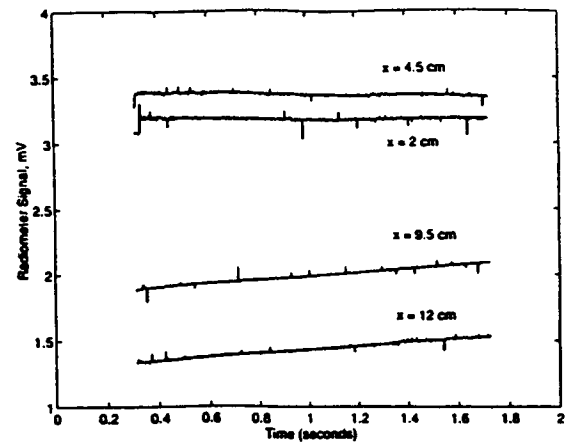


Fig. 5. Measured global radiometer signals during the final 1.5 seconds of the drop for different axial locations. The radial location is 10 cm from the flame centerline. Time $t = 0$ in the plot corresponds to 3.3 seconds after commencement of the drop.

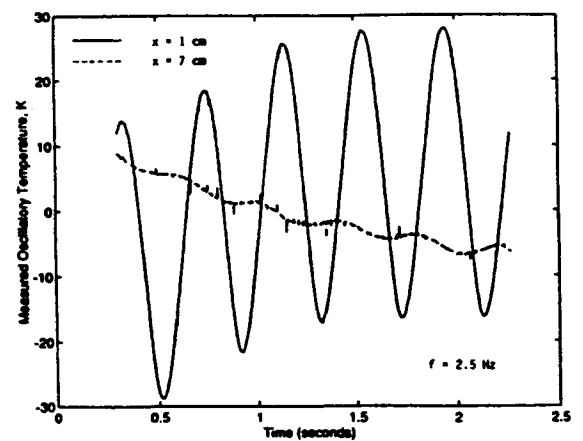


Fig. 7. Oscillatory component of centerline temperature at two axial locations for a microgravity propane flame at 2 cc/sec. The iris frequency was 2.5 Hz. The data is for the final 2 seconds of the drop.

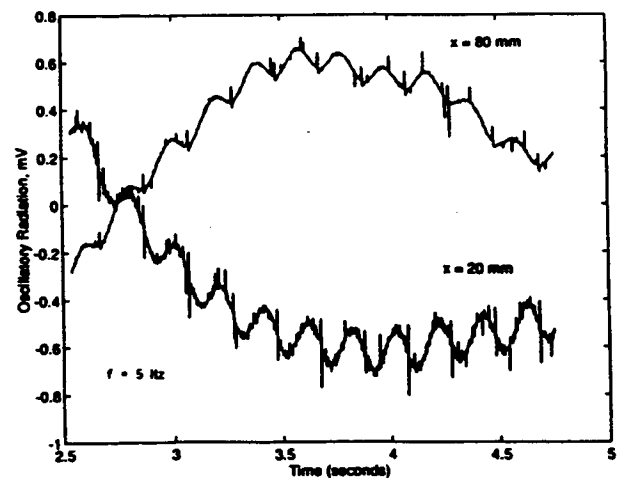


Fig. 9. Oscillatory component of slice-radiometer signal at two axial locations for a radial location of 10 cm; microgravity propane flame at 2 cc/sec; iris frequency = 5.0 Hz.